Full paper presented at MDA2016 Conference

Geometry optimization of a magnetorheological clutch operated by coils

Francesco Bucchi, Paola Forte, Francesco Frendo

Department of Civil and Industrial Engineering

Università di Pisa

Largo Lucio Lazzarino, 56122 - Pisa, Italy

Abstract

Magnetorheological fluids (MRFs) are smart materials responsive to magnetic field, widely applied in dampers and shock absorbers but also in clutches and brakes. The MRF gap shape is a very important topic in the design of clutches, since it directly influences the transmissible torque and the power loss.

In this paper an approach to MRF clutch design based on optimization is proposed and tested on four different layouts. Starting from a given available volume, two MRF gap shapes, namely single cylinder and multi-disc, and two coils positions, i.e. internal or external, were considered. A lumped parameter model was developed to analytically compute the magnetic flux along the clutch magnetic circuit and to calculate the transmissible torque of the clutch.

The optimal geometry of the clutch for maximum transmissible torque, in terms of number and dimensions of the coil sectors, was determined for each shape and coil configuration and the results were validated by finite element models.

1 Introduction

Magnetorheological fluids (MRFs) are smart materials having several applications in research and industry. The main peculiarity is the capability to change their apparent viscosity and to exhibit a variable yield shear stress if subject to magnetic field. If the magnetic field is not applied, MRFs behave like Newtonian fluids, while under the effect of magnetic field they exhibit a visco-plastic characteristic which is usually modeled either by the Bingham-plastic [1] or the Herschel-Bulkley [2] models. MRFs are made of a carrier fluid, which is usually oil, having micrometric ferromagnetic particles dispersed right inside. In the absence of magnetic field, the ferromagnetic particles are randomly dispersed, while if the fluid is crossed by magnetic field, the ferromagnetic particles align themselves along the magnetic field and confer to the MRF a higher shear strength. As stated by suppliers [3], the time needed to change the particles orientation upon the application, or the removal, of the magnetic field is less than five milliseconds, as confirmed also in [4], while some studies regarding real MRF devices assess the response time is strongly variable in the range 0.01–1.2 s [5]– [6].

Even though the first MRFs applications date back to the late 1940s – early 1950s, when the first magnetorheological clutches operated by coils were designed and patented by Rabinow [7, 8], the research activity grew up recently [9–11] thanks to the availability of commercial MRFs and to the spread of Finite Element (FE) software, which can accurately compute the magnetic field distribution in complex geometries.

A widely diffused application of MRFs is related to damping, mainly in vehicle shock absorbers [12–15] but also in civil constructions [16]. An alternative application is related to clutches and brakes [17, 18], usually composed by two parts, both rotating in the case of clutches or one fixed and one rotating in the case of brakes; the gap between the two parts is filled with MRF.

The MRF gap shape is a very important topic in the design of the clutch, since it directly influences the magnetic field distribution, the transmissible torque and the power loss. Usually clutches and brakes have planar (disc) or cylindrical shape gaps [19] and the magnetic field is generated by coils, even if the use of permanent magnets is sometimes considered [20–22]. In particular, the authors faced with the development of magnetorheological clutches conceived in order to transmit high torque in engaged configuration under strict size constraints [23, 24]. They developed several clutch models [25] where the MRF gap and the whole clutch geometry was obtained in an iterative way.

In the literature the MRF gap geometry is also studied by means of optimization algorithms. In Karakoc [26] the optimization study aimed at maximizing the transmissible torque of a multidisc MRF brake excited by coils, having the number of discs and the coil position (external) fixed and the external diameter subject to constraint. More recently, Nguyen and Choi published several papers on MRF clutch and brake optimization [27–31] using both FEM and lumped parameters approaches. In particular, they optimized the transmissible torque considering single disc, multi-disc and T-shaped fluid gaps arrangements under the constraints of size, mass and temperature due to friction in the case of no magnetic field.

In this paper an alternative approach to MRF clutch design based on optimization is proposed. The aim of the activity was to found the optimal clutch layout and the optimal clutch dimensions in order to maximize the transmissible torque in engaged condition without clutch slip, given the available cylindrical volume. For this reason two MRF gap shapes, namely single cylinder and multi-disc, and two different coil positions, namely internal and external, were considered. A lumped parameter model was developed to analytically simulate the magnetic flux density along the magnetic circuit and, consequently, the transmissible torque of the clutch. The optimal geometry of the clutch was determined for each shape and coil configuration and the results were validated by FEM models. The resulting optimal clutch could be used for several applications where the engagement and disengagement of mechanical devices, e.g. auxiliaries in internal combustion engines [], is required.

2 MRF clutches layout

Four clutch layouts were considered in this analysis, as shown in Fig. 1. In particular, Fig. 1a and Fig. 1b represent the cross section of two clutches having cylindrical gap, while Fig. 1c and Fig. 1d represent the transversal section of two clutches having a multidisc gap. Each layout is made up of two rotor parts, while the coil sectors are nestled in internal or external stators, in order to avoid the use of brush contacts. The rotors can be made up of ferromagnetic or non-ferromagnetic materials; in the case of a rotor composed of both ferromagnetic and non-ferromagnetic materials, these can be joined by welding even if the clutch complexity increases. The ferromagnetic and non-ferromagnetic sectors were determined in order to guarantee suitable ferromagnetic circuits (see Section 3), while the number and dimensions of the coil sectors were left to be determined by the optimization algorithm. The geometries shown in Fig. 1 have to be considered as schematic

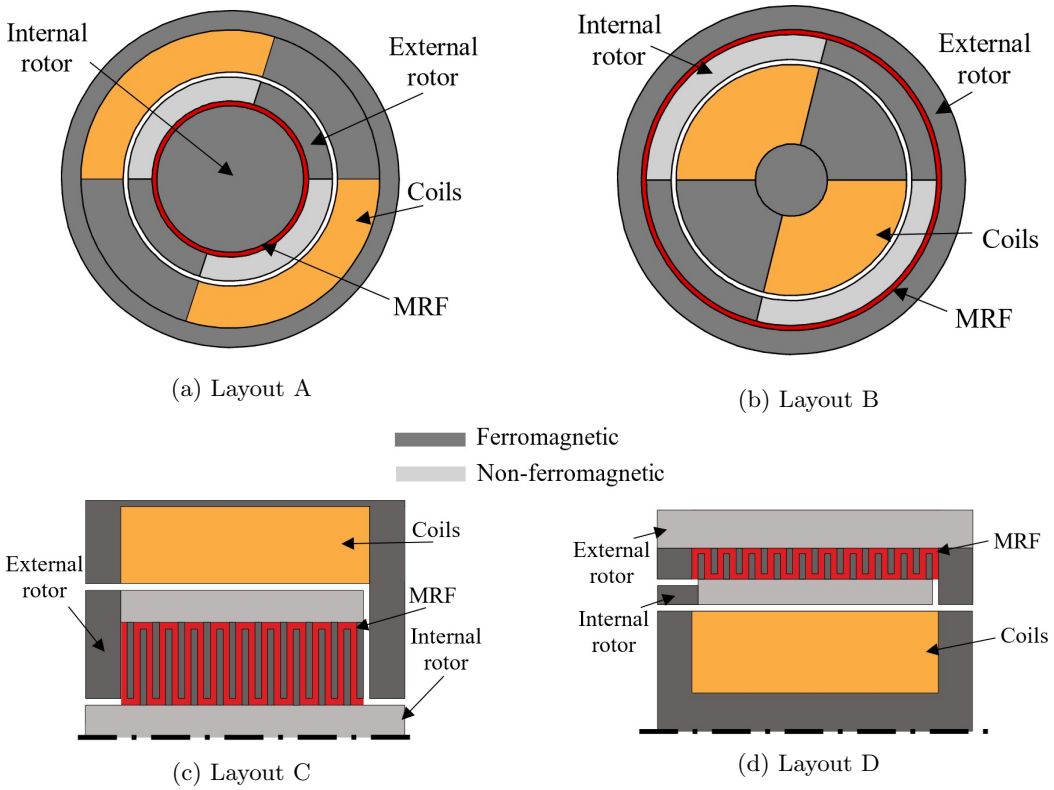

(a) Layout A

(b) Layout B

(c) Layout C

(d) Layout D

Figure 1: MRF clutch layouts: a) single cylinder with external coils, b) single cylinder with internal coils, c) multidisc with external coils, d) multidisc with internal coils

simplified representations since, beyond the sectors dimensions, even the number of coil sectors in the cylindrical layout and the number of discs in the multidisc layout cannot be known a-priori.

The first layout (Fig. 1a) presents an internal rotor element, fully ferromagnetic, and an external rotor element made up of alternating ferromagnetic and non-ferromagnetic materials. The rotors are separated by MRF and the coils are placed externally. The second layout (Fig. 1b) presents an external fully ferromagnetic rotor element and an internal rotor element made up of alternating ferromagnetic and non-ferromagnetic materials; the coils are placed internally.

The third and fourth layouts (Fig. 1c-1d) both present an internal rotor element composed by a non-ferromagnetic shaft having a series of ferromagnetic plates fixed on it. The external rotor element is made up of juxtaposed ferromagnetic plates and non-ferromagnetic hollow cylinder. The only difference is related to the coils position, which are external in Layout C and internal in Layout D.

The size constraints considered for each layout are listed in Tab. 1. The external diameter and the length were defined in order to compare the results with a MRF clutch prototype already

External diameter	74 mm
Length	50 mm
MRF gap thickness	1 mm
Minimum metal plate thickness	1 mm

Table 1: Size and technological constraints

developed by the authors [24], which was equipped with a permanent magnet. The MRF gap thickness and the minimum metal place thickness were fixed to 1 mm due to technological issues. Also the minimum thickness of non-ferromagnetic hollow cylinder and shaft (e.g. internal rotor shaft in Layout C) were chosen on the basis of mechanical structural consideration based on the stress of the parts involved in the torque transmission. It is worth noting that such geometric parameters could not be determined by the optimization procedure since these are non ferromagnetic and consequently they do not directly affect the magnetic circuit.

3 Lumped parameter model of the clutch

The magnetic circuits were defined considering the following assumptions:

1. all the magnetic field lines form closed loops, flowing around each coil sector, which pass through ferromagnetic parts and magnetorheological fluids;
2. the reluctance of the circuit elements are considered as lumped parameters and are determined considering the relative permeability, defined as $\mu_R = \frac{B}{H\mu_0}$, of the MRF (μ_R^{MR}, Lord Corporation MRF 140 CG) and of the iron parts (μ_R^{Fe}, AISI1018) starting from the B-H curves shown in Fig. 2;
3. the non-ferromagnetic parts are assumed to have $\mu_R = 1$;
4. each coil sector generates the magnetomotive force $\mathcal{F} = N\,I$, where N is the number of coils belonging to each sector and I is the current flowing in each coil wire;
5. on the basis of the Hopkinson's law, $\mathcal{F} = \Phi\ R$, where Φ is the magnetic flux and R is the reluctance of the circuit.

The reluctance of the circuit was then determined considering the above mentioned hypotheses and the geometrical properties of each layout.

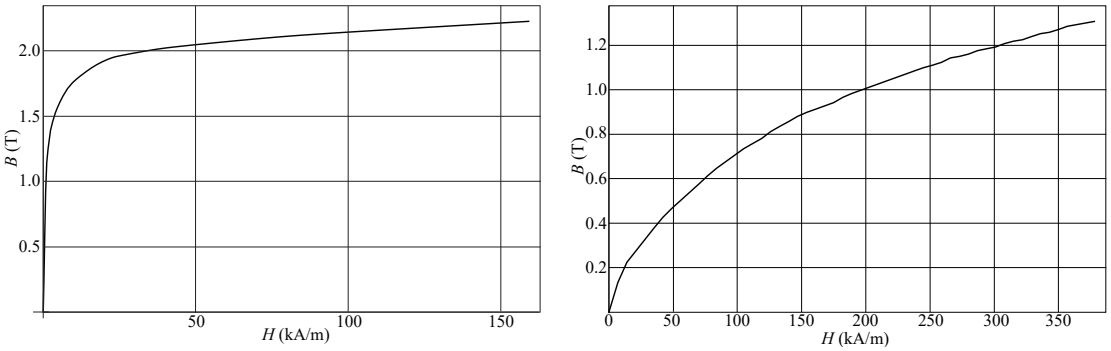

(a) 1a (b) 1b

Figure 2: Ferromagnetic iron and MRF B-H curves.

3.1 Layout A

Considering the planar model shown in Fig. 1a (dimensions given in Fig. 3a and length $L = 50$ mm), it is possible to find the minimum reluctance path of the magnetic field around each coil, which is schematically represented by the green lines in Fig. 3b. If the reluctance of the air and MRF areas crossed by the magnetic field are considered as lumped parameters and the reluctance of the ferromagnetic iron is mainly due to the external hollow cylinder of the clutch, it is possible to describe the magnetic circuit associated to the clutch with the scheme proposed in Fig. 3c.

The magnetomotive force $\mathcal{F}^A$ is computed on the basis the number of coils N^A and the current I flowing in each coil. The number of coils is given by the ratio between the coil sector area A_C^A and the coil wire radius $r_w = 1$ mm multiplied by wire packaging factor f_p= 0.75 and

$$\mathcal{F}^A = N^A I = \frac{A_C^A}{\pi r_w^2} f_p I = \frac{\pi \left[\left(r_3^A\right)^2 - \left(r_2^A + s\right)^2\right] \frac{(2\pi - n^A \alpha^A)}{2\pi n^A}}{\pi r_w^2} f_p I \tag{1}$$

where r_2^A, $r_3^A$and α^A are shown in Fig. 3a, $s = 1$ mm is the MRF and air gap thickness and n^A is the number of coil sectors. It is worth noting that the magnetomotive force generated by a single coil is split along two opposite paths; for this reason the equivalent reluctance of the circuit is

$$R_{eq}^A = \left[2\left(R_{Air}^A + R_{MR}^A + R_{Fe}^A\right)\right]/2, \tag{2}$$

where $R_{Air}^A = \frac{s}{(r_2^A + s/2)\alpha^A L}$, $R_{MR}^A = \frac{s}{\mu_R^{MR}(r_1^A + s/2)\alpha^A L}$ and $R_{Fe}^A \approx \frac{\left(\frac{2\pi}{n^A} - \alpha^A\right)\left(r_3^A + r_4^A\right)}{4\mu_R^{Fe}\left(r_4^A - r_3^A\right)L}$.

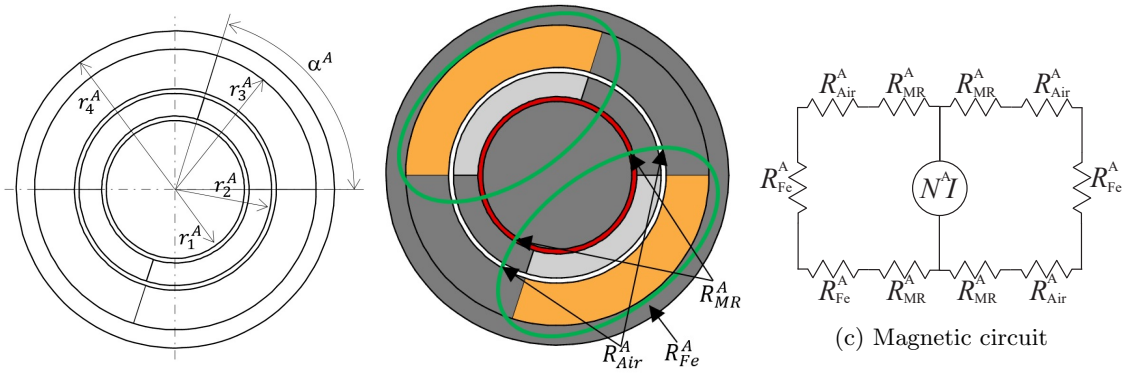

(a) Dimensions

(b) Magnetic flux lines drawing

(c) Magnetic circuit

Figure 3: Layout A characteristics.

The magnetic flux Φ^A is then computed as

$$\Phi^A = \frac{N^A\, I}{R^A_{eq}} \tag{3}$$

and consequently the magnetic fields B^A_{Fe} and B^A_{MR} are computed as follows

$$B^A_{Fe} = \frac{\Phi^A}{2(r_4^A - r_3^A)L} \tag{4}$$

$$B^A_{MR} = \frac{\Phi^A}{(r_1^A - \frac{s}{2})\alpha^A L} \tag{5}$$

The magnetic field H^A_{Fe} and H^A_{MR} are finally computed as

$$H^A_{Fe} = \frac{B^A_{Fe}}{\mu_R^{Fe}\mu_0} \tag{6}$$

$$H^A_{MR} = \frac{B^A_{MR}}{\mu_R^{MR}\mu_0} \tag{7}$$

It is worth noting that the relative permeabilities μ_R^{Fe} and μ_R^{MR} are functions of the magnetic field H^A_{Fe} and H^A_{MR} respectively and they are computed starting from the materials B-H curves. Since the magnetic field is the output of the analysis and the relative permeabilities are used to compute it, the problem is implicit. For this reason a numerical algorithm which computes the magnetic field iteratively was implemented. Similarly in [29, 31] the relative permeability of the materials was computed during the optimization process by the FEM sofware.

3.2 Layout B

Similarly to the analysis carried out for the Layout A, the magnetic circuit related to Layout B, the dimensions of which are shown in Fig. 4a, is derived as shown in Fig. 4b-4c.

The magnetomotive force $\mathcal{F}^B$is given by

$$\mathcal{F}^B = N^B I = \frac{A_C^B}{\pi r_w^2}\, f_p I = \frac{\pi\left[\left(r_2^B\right)^2 - \left(r_1^B\right)^2\right]\frac{(2\pi - n^B\alpha^B)}{2\pi n^B}}{\pi r_w^2} f_p I \tag{8}$$

and the equivalent reluctance is formally the same way as in Layout A, since the equivalent magnetic circuit is composed by the same lumped elements. The only difference is related to the position of air reluctance and MRF which have reverse order. However, the different order does not affect the equivalent reluctance because air and MRF reluctance are in series. Therefore

$$R_{eq}^B = \left[2\left(R_{Air}^B + R_{MR}^B + R_{Fe}^B\right)\right]/2, \tag{9}$$

where $R_{Air}^B = \frac{s}{(r_2^B + s/2)\alpha^B L}$, $R_{MR}^B = \frac{s}{\mu_R^{MR}(r_3^B + s/2)\alpha^B L}$ and $R_{Fe}^B \approx \frac{\left(\frac{2\pi}{n^B} - \alpha^B\right)\left(r_3^B + r_4^B\right)}{4\mu_R^{Fe}\left(r_4^B - r_3^B\right)L}$.

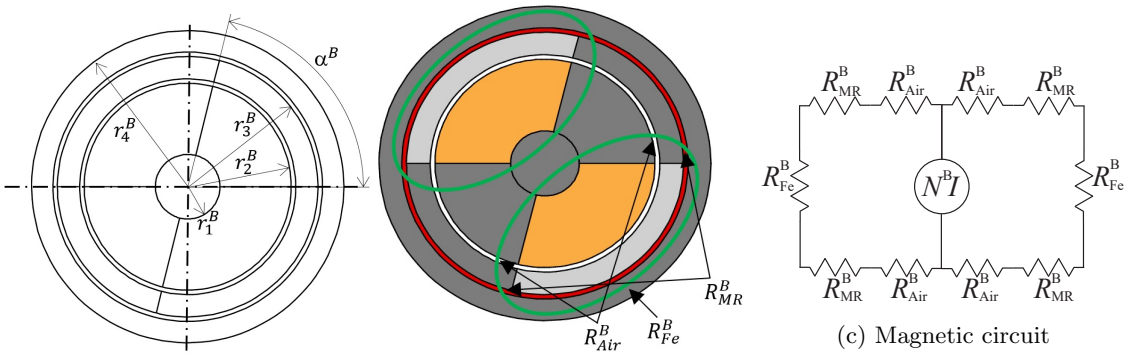

(a) Dimensions

(b) Magnetic flux lines drawing

(c) Magnetic circuit

Figure 4: Layout B characteristics.

The magnetic flux Φ^B is then computed as

$$\Phi^B = \frac{N^B\, I}{R_{eq}^B} \tag{10}$$

and consequently the magnetic fields B_{Fe}^B and$B\ {}_{MR}^{A}$ are computed as follows

$$B_{Fe}^B = \frac{\Phi^B}{2(r_4^B - r_3^B)L} \tag{11}$$

$$B^B_{MR} = \frac{\Phi^B}{(r^B_3 - \frac{s}{2})\alpha^B L} \tag{12}$$

The magnetic field H^B_{Fe} and H^B_{MR} are finally computed as

$$H^B_{Fe} = \frac{B^B_{Fe}}{\mu^{Fe}_R \mu_0} \tag{13}$$

$$H^B_{MR} = \frac{B^B_{MR}}{\mu^{MR}_R \mu_0} \tag{14}$$

where the relative permeability values were chosen as for Layout A clutch.

3.3 Layout C

Also for Layout C, the magnetic circuit was drawn as shown in Fig. 5a-5c.

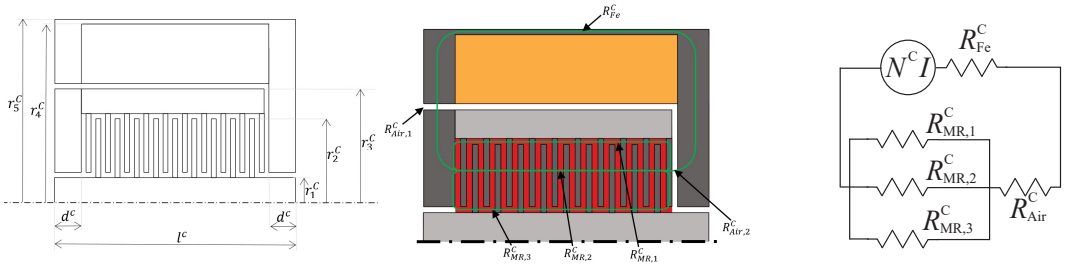

(a) Dimensions

(b) Magnetic flux lines drawing

(c) Magnetic circuit

Figure 5: Layout C characteristics.

The magnetomotive force $\mathcal{F}^C$is given by

$$\mathcal{F}^C = N^C I = \frac{A^C_C}{\pi r^2_w} f_p I = \frac{[r^C_4 - (r^C_3 + s)](l^C - 2d^C)}{\pi r^2_w} f_p I \tag{15}$$

and the equivalent reluctance is given by the series of the reluctance of the air gaps $R^C_{Air,1}$and $R^C_{Air,2}$ and the reluctance of MRF R^C_{MRF}. In this case, the reluctance of the MRF was split in three parts, since three different parallel reluctance paths, shown in Fig. 5b-5c, can be identified even in a lumped parameters analysis. For this reason R^C_{MRF} is obtained as

$$(R^C_{MR})^{-1} = (R^C_{MR,1})^{-1} + (R^C_{MR,2})^{-1} + (R^C_{MR,3})^{-1} \tag{16}$$

with

$$R^C_{MR,1} = \frac{3s\ n^C}{\pi\mu^{MR}_R((r^C_2+s)^2-(r^C_2)^2)} \tag{17}$$

$$R^C_{MR,2} = \frac{2s\ n^C}{\pi\mu^{MR}_R((r^C_2)^2-(r^C_1+s)^2)} \tag{18}$$

$$R^C_{MR,3} = \frac{3s\ n^C}{\pi\mu^{MR}_R((r^C_1+s)^2-(r^C_1)^2)} \tag{19}$$

where n^C is the number of disc plates and the dimensions are identified in Fig. 5b. The equivalent magnetic circuit reluctance is then

$$R^C_{eq} = R^C_{MR} + R^C_{Air,1} + R^C_{Air,2} + R^C_{Fe} \tag{20}$$

where $R^C_{Air,1} = \frac{s}{\pi((r^C_2+s)^2-(r^C_1)^2)}$, $R^C_{Air,2} = \frac{s}{2\pi(r^C_3+s/2)d^C}$ and $R^B_{Fe} \approx \frac{l^C-2d^C}{\pi\mu^{Fe}_R((r^C_5)^2-(r^C_4)^2)}$.

The magnetic flux Φ^C is then computed as

$$\Phi^C = \frac{N^C\ I}{R^C_{eq}} \tag{21}$$

and consequently the magnetic fields B^C_{Fe} and$B\ ^C_{MR}$ are computed as follows

$$B^C_{Fe} = \frac{\Phi^C}{\pi\left((r^C_5)^2-(r^C_4)^2\right)} \tag{22}$$

$$B^C_{MR} = \frac{\Phi^C}{\pi\left((r^C_2)^2-(r^C_1+s)^2\right)} \frac{R^C_{MR,1}R^C_{MR,3}}{\left(R^C_{MR,1}R^C_{MR,2}+R^C_{MR,1}R^C_{MR,3}+R^C_{MR,2}R^C_{MR,3}\right)} \tag{23}$$

where the magnetic flux density in the MRF B^C_{MR} was computed considering only the magnetic flux along the central path of the parallel circuit portion shown in Fig. 5c. This is due to the fact that the transmitted torque is related to the magnetic field in the MRF between facing discs, which corresponds to the central part of the magnetic field path.

The magnetic field H^C_{Fe} and H^C_{MR} are finally computed as

$$H^C_{Fe} = \frac{B^C_{Fe}}{\mu^{Fe}_R\mu_0} \tag{24}$$

$$H^C_{MR} = \frac{B^C_{MR}}{\mu^{MR}_R\mu_0} \tag{25}$$

where the relative permeabilities where numerically found as previously described.

3.4 Layout D

Finally Layout D clutch was defined as shown in Fig. 6a-6c and the magnetic circuit was drawn as shown in Figure 6c.

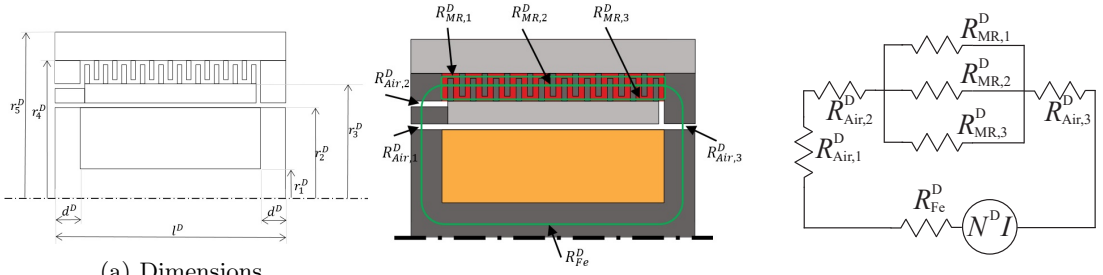

(a) Dimensions

(b) Magnetic flux lines drawing

(c) Magnetic circuit

Figure 6: Layout D characteristics.

The magnetomotive force $\mathcal{F}^D$is given by

$$\mathcal{F}^D = N^D I = \frac{A_C^D}{\pi r_w^2} f_p I = \frac{(r_2^D - r_1^D)(l^D - 2d^D)}{\pi r_w^2} f_p I \tag{26}$$

and, as similarly to layout C, the equivalent reluctance is given by the series of the reluctance of the air gaps $R^D_{Air,1}$, $R^D_{Air,2}$ and $R^D_{Air,3}$ and the reluctance of MRF R^D_{MR}. Also in this case, the reluctance of the MRF was split in three parts and R^D_{MR} can be obtained as

$$(R^D_{MR})^{-1} = (R^D_{MR,1})^{-1} + (R^D_{MR,2})^{-1} + (R^D_{MR,3})^{-1} \tag{27}$$

with

$$R^D_{MR,1} = \frac{3s\ n^D}{\pi \mu_R^{MR}((r_4^D)^2 - (r_4^D - s)^2)} \tag{28}$$

$$R^D_{MR,2} = \frac{2s\ n^D}{\pi \mu_R^{MR}((r_4^D - s)^2 - (r_3^D + s)^2)} \tag{29}$$

$$R^D_{MR,3} = \frac{3s\ n^D}{\pi \mu_R^{MR}((r_3^D + s)^2 - (r_3^D)^2)} \tag{30}$$

where n^D is the number of disc plates and the dimensions are identified in Figure 5c. The

equivalent magnetic circuit reluctance is then

$$R_{eq}^{D} = R_{MR}^{D} + R_{Air,1}^{D} + R_{Air,2}^{D} + R_{Air,3}^{D} + R_{Fe}^{D} \tag{31}$$

where $R_{Air,1}^{D} = R_{Air,3}^{D} = \frac{s}{2\pi(r_2^D+s)d^D}$, $R_{Air,2}^{C} = \frac{s}{2\pi(r_3^D+s)d^D}$ and $R_{Fe}^{B} \approx \frac{l^D-2d^D}{\pi\mu_R^{Fe}\left(r_1^D\right)^2}$.

The magnetic flux Φ^D is then computed as

$$\Phi^D = \frac{N^D\, I}{R_{eq}^{D}} \tag{32}$$

and consequently the magnetic fields B_{Fe}^{D} and$B\ _{MR}^{D}$ are computed as follows

$$B_{Fe}^{D} = \frac{\Phi^D}{\pi\left(r_1^D\right)^2} \tag{33}$$

$$B_{MR}^{D} = \frac{\Phi^D}{\pi\left(\left(r_4^D - s\right)^2 - \left(r_3^D + s\right)^2\right)} \frac{R_{MR,1}^{D} R_{MR,3}^{C}}{\left(R_{MR,1}^{D} R_{MR,2}^{C} + R_{MR,1}^{D} R_{MR,3}^{D} + R_{MR,2}^{D} R_{MR,3}^{D}\right)} \tag{34}$$

where, analogously to Layout c) clutch, the magnetic flux density in the MRF B_{MR}^{D} was computed considering only the magnetic flux along the central path of the parallel circuit portion shown in Fig. 6b. The magnetic field H_{Fe}^{D} and H_{MR}^{D} are finally computed as

$$H_{Fe}^{D} = \frac{B_{Fe}^{D}}{\mu_R^{Fe}\mu_0} \tag{35}$$

$$H_{MR}^{D} = \frac{B_{MR}^{D}}{\mu_R^{MR}\mu_0} \tag{36}$$

where the relative permeabilities where numerically found as previously described.

4 Torque computation

The transmissible torque of each clutch layout was computed starting from the knowledge of the magnetic field along the MRF gap. Since the focus was on the transmissible torque without clutch slip, only the contribution of the yield shear stress, the profile of which is given in Fig. 7 as a function of the magnetic field intensity H, was considered, neglecting the viscous term. The yield stress curve refers to room temperature but it is known [32] that the temperature influences the yield shear stress of the MRF. In particular higher temperature values negatively affects the yield

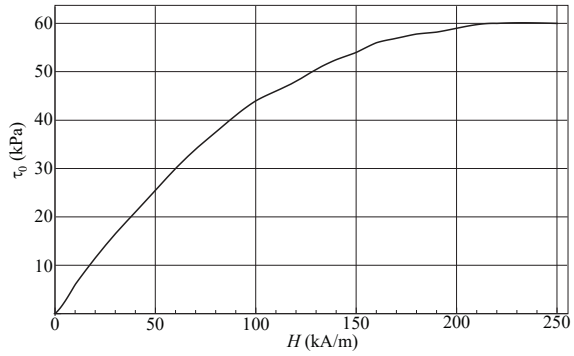

Figure 7: Yield stress versus magnetic field intensity - Lord Corporation MRF 140CG

stress capability of the MRF. For this reason the absence of clutch slip is desired in engaged condition since no heat is generated due to MRF work. However also the current flowing in the coils contributes to the heat generation in engaged condition and this contribution was neglected in this analysis. The correctness of this assumption was verified a posteriori, computing, for each optimal clutch geometry, the heat generated by the current which resulted lower than 20 W.

In Layout A and Layout B, since the magnetic field H^A and H^B was assumed constant in the portions of the MRF gap crossed by magnetic flux, having angular dimension α^A and α^B (see Fig. 3 and Fig. 4), and zero elsewhere, the yield shear stress was consequently assumed constant and equal to $\tau_0(H)$ in the portions of the MRF gap crossed by the magnetic flux and zero in the portions of the MRF gap which are not subjected to the magnetic flux.

In Layout C and Layout D, the annular area of the discs which contributes to the torque transmission was identified considering the zones where the primary and secondary discs face one against the other, i.e. between $r_1^C + s$ and r_2^C in Layout C and between $r_3^D + s$ and $r_4^D - s$ in Layout D (see Fig. 5 and Fig. 6).

Considering the equations given in [23], the transmissible torque for each layout is

$$T^A(H^A) = n^A \alpha^A L (r_1^A)^2 \tau_0(H^A) \tag{37}$$

$$T^B(H^B) = n^B \alpha^B L (r_3^B)^2 \tau_0(H^B) \tag{38}$$

$$T^C\left(H^C\right) = 4\pi n^C \tau_0(H^C) \frac{(r_2^C)^3 - (r_1^C + s)^3}{3} \tag{39}$$

$$T^D\left(H^D\right) = 4\pi n^D \tau_0(H^D) \frac{(r_4^D - s)^3 - (r_3^D + s)^3}{3} \tag{40}$$

5 Optimization

In order to find the geometrical parameters and the number of coil sectors (or the number of discs) that maximize the transmissible torque, an optimization procedure is due. It is worth noting that the effect of many parameters is not easily predictable, since they affect in a complex way the magnetomotive force, the circuit reluctance and the torque tranmission. For example, considering Layout A and Layout B, if the angular sector of the MRF crossed by magnetic flux (α^A and α^B) is increased, the mangetomotive force decreases (the coil sectors area is reduced) as well as the reluctance of the air and MRF decreases too; in addition the zone of the MRF which contributes to the torque transmission is wider. For this reason it is not easily predictable how to find the optimal value without using optimization algorithms.

5.1 Algorithm description

The optimum clutch geometry was computed following the conceptual scheme presented in Fig. 8. For the sake of conciseness the scheme refers only to Layout A clutch but can be easily transposed to the other clutch layouts.

The first step of the procedure consists in manually guessing the initial values of the optimization parameters, which are, in the considered example, r_1^A, r_2^A, r_3^A, α^A. Then a *for* loop is initiated where the number of coils sectors n^A is the index variable.

The external dimensions values are also considered and the magnetic fields in the MRF and in the iron parts is computed on the basis of the model presented in Section 3.1. Then a series of constraint checks is performed considering both the saturation of the ferromagnetic iron parts ($H_{Fe,sat} = 1.4$ T) and the geometrical consistency (e.g. $r_3^A > r_2^A > r_1^A$). If the constraints are satisfied, the transmissible torque is computed, otherwise a new set of geometry parameters is guessed.

The Nelder-Mead algorithm [33] is used to generate the new set of parameters at each step, until the convergence at the optimal solution is reached and the accuracy of the solution meets the minimum criteria.

Once the optimal solution is found for a given number of coils sectors n^A (or the optimal number of disc plates for layouts C and D), the optimal torque value $\overline{T}_n^A$ is stored and the *for* loop iterates changing the number of coils sectors (or the number of discs for Layout C and D). Finally, the maximum value of the transmissible torque $\overline{T}^A$, related to the optimal number of coils sectors

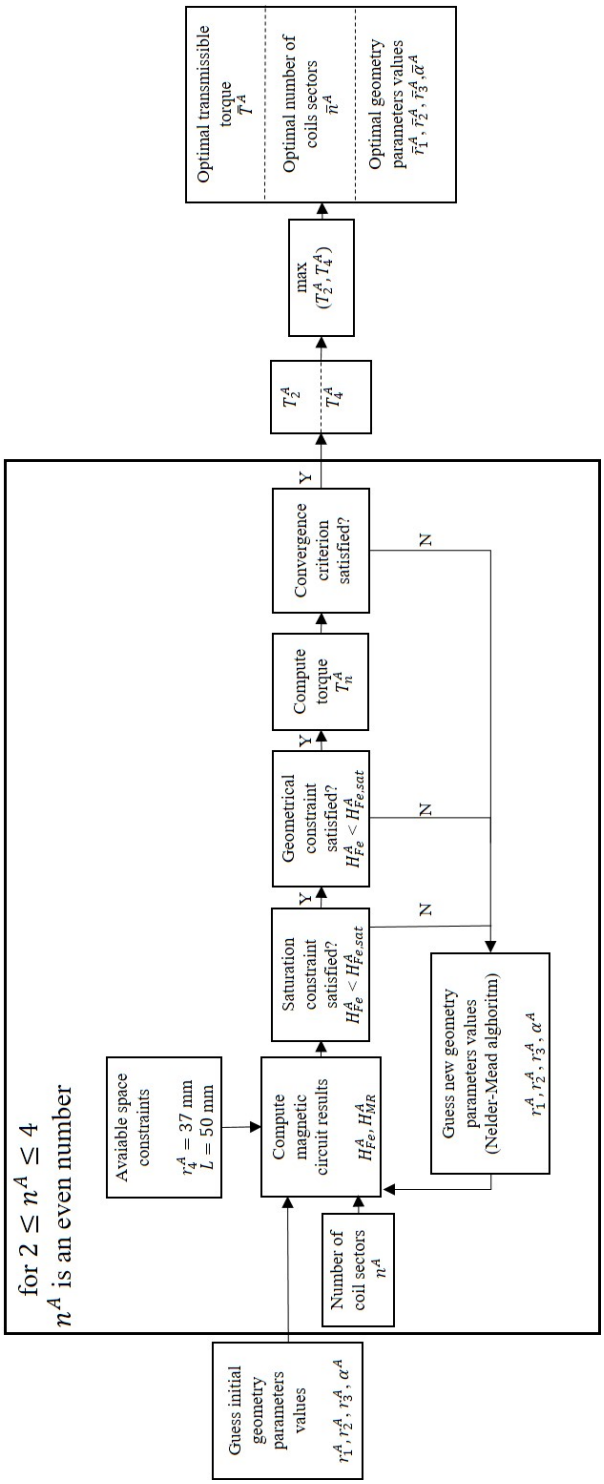

Figure 8: Optimization conceptual scheme

Layout A		Layout B		Layout C		Layout D	
$\overline{T}^A$(Nm)	0.91	$\overline{T}^B$(Nm)	1.87	$\overline{T}^C$(Nm)	2.11	$\overline{T}^D$(Nm)	5.49
$\overline{n}^A$ (-)	2	$\overline{n}^B$ (-)	2	$\overline{n}^C$ (-)	10	$\overline{n}^D$ (-)	10
$\overline{r}_1^A$ (mm)	15.1	$\overline{r}_1^B$ (mm)	7.2	$\overline{r}_1^C$ (mm)	5	$\overline{r}_1^D$ (mm)	6.7
$\overline{r}_2^A$ (mm)	21.1	$\overline{r}_2^B$ (mm)	23.2	$\overline{r}_2^C$ (mm)	16.8	$\overline{r}_2^D$ (mm)	20.7
$\overline{r}_3^A$ (mm)	31.2	$\overline{r}_3^B$ (mm)	29.2	$\overline{r}_3^C$ (mm)	22.8	$\overline{r}_3^D$	26.7
$\overline{\alpha}^A$ (deg)	70.3	$\overline{\alpha}^B$ (deg)	75.9	$\overline{r}_4^C$ (mm)	36	$\overline{r}_4^D$ (mm)	32
				$\overline{d}^C$(mm)	5.5	$\overline{d}^D$(mm)	5.5
$\overline{H}_{MR}^A$ (kA/m)	63.3	$\overline{H}_{MR}^B$ (kA/m)	38.8	$\overline{H}_{MR}^C$ (kA/m)	18.9	$\overline{H}_{MR}^D$ (kA/m)	27.4
$\overline{B}_{MR}^A$ (T)	0.56	$\overline{B}_{MR}^B$ (T)	0.34	$\overline{B}_{MR}^C$ (T)	0.26	$\overline{B}_{MR}^D$ (T)	0.31
$\overline{N}^A$	308	$\overline{N}^B$	293	$\overline{N}^C$	314	$\overline{N}^D$	362

Table 2: Optimal parameters.

$\overline{n}^A$ and to the optimal geometry parameters $\overline{r}_1^A$, $\overline{r}_2^A$, $\overline{r}_3^A$,$\overline{\alpha}^A$, is chosen among the maximum values obtained at each loop.

5.2 Optimization results

The results listed in Tab. 2 were obtained considering the maximum current $I = 3$ A.

Either for the cylindrical and for the multidisc layouts, the most promising geometry, in terms of transmissible torque, are those having coils in the internal zone of the clutch and the MRF gap externally. This result could be reasonably expected since the torque rises in a more than proportional way with the MRF gap radius. In particular, the Layout D clutch is able to transmit the higher torque, the value of which is 5.49 Nm. In addition, for cylindrical gap layouts, the optimal number of coil sectors, i.e. $\overline{n}^A$ and $\overline{n}^B$, is 2, while for multidisc layouts, the optimal number of disc plates is 10 in both cases.

Beyond the optimal value, a sensitive analysis to the number of coil sectors in Layout A and to the number of disc plates for Layout C was also performed. Concerning Layout A, the torque monotonically decreases as the number of coil sectors rises. On the contrary, Layout D presented a maximum torque value for 10 disc plates and the torque was found to decrease either if the number of the plates was increased or decreased. This is probably due to the fact that, among many others, two important opposite effects contribute to the torque computation as the number of disc plates changes. Indeed, if $\overline{n}^C$ is increased, the number of active surfaces able to transmit the torque rises (see Eq. 39), but also the reluctance of the MRF rises (see Eq. 16) and, consequently, the magnetic flux density in the fluid is lower and the yield shear stress of the fluid decreases too.

6 FEM validation

For each optimal layout, a magnetic finite element model was developed using FEMM software [34] in order to validate the results found in the optimization procedure. The software is considered a reliable freeware intrument to perform planar and axis-symmetric analyses and it is widely used in the literature and in the industry, as discussed in [35]. In particular, the aim of the model was to verify that, for each optimal clutch geometry, the results found using the simplified lumped parameters model were similar to the more accurate ones found using a finite element model. In particular, the comparison was made in terms of magnetic flux density within the MRF area.

The FEM model made use of the non-linear B-H curve shown in Fig. 2, both for MRF and for ferromagnetic AISI1018, while for air and non ferromagnetic parts the relative permeability was set to 1. The coils were modeled using copper characteristics and the number of turns was set, for each model, in accordance to Tab. 2. Concerning Layout A and Layout B a planar model was developed, while for Layout C and Layout D an axisymmetric model was used.

The results of the FEM analysis are shown in Fig. 9.

In Layout A and Layout B models the magnetic flux lines follows the magnetic circuit guessed in Fig. 3b and Fig. 4b and they do not cross the external air area. The average magnetic field density in the fluid crossed by magnetic field lines is 0.51 T and 0.29 T for Layout A and Layout B respectively. Concerning Layout C and, especially, Layout D, some magnetic flux lines come out from the magnetic field circuit guessed in Fig. 6b and flow in the air. The average magnetic field density in the MRF is 0.31 T and 0.17 T for Layout C and Layout D respectively.

Table 3 shows the comparison between the results obtained with the lumped parameter model used for the optimization and the results obtained by the FEM analysis. Concerning Layout A and Layout B the lumped parameter model overestimates the magnetic field in the fluid, and consequently the transmitted torque of about 10%. On the contrary in Layout C the magnetic field density is underestimated of about 10%. Due to simplifications introduced by the lumped model, these results are considered satisfactory. Indeed, the optimization model allows the designer to recognize the magnetic field circuit and to choose the optimal geometrical solution in very short time, taking into account many opposite and differently weighted effects.

The results obtained for Layout D) using the lumped parameters and the FEM model are strongly different. This is due to the fact that the actual magnetic circuit found with the FEM model is significantly different from the one guessed to develop the lumped parameter model.

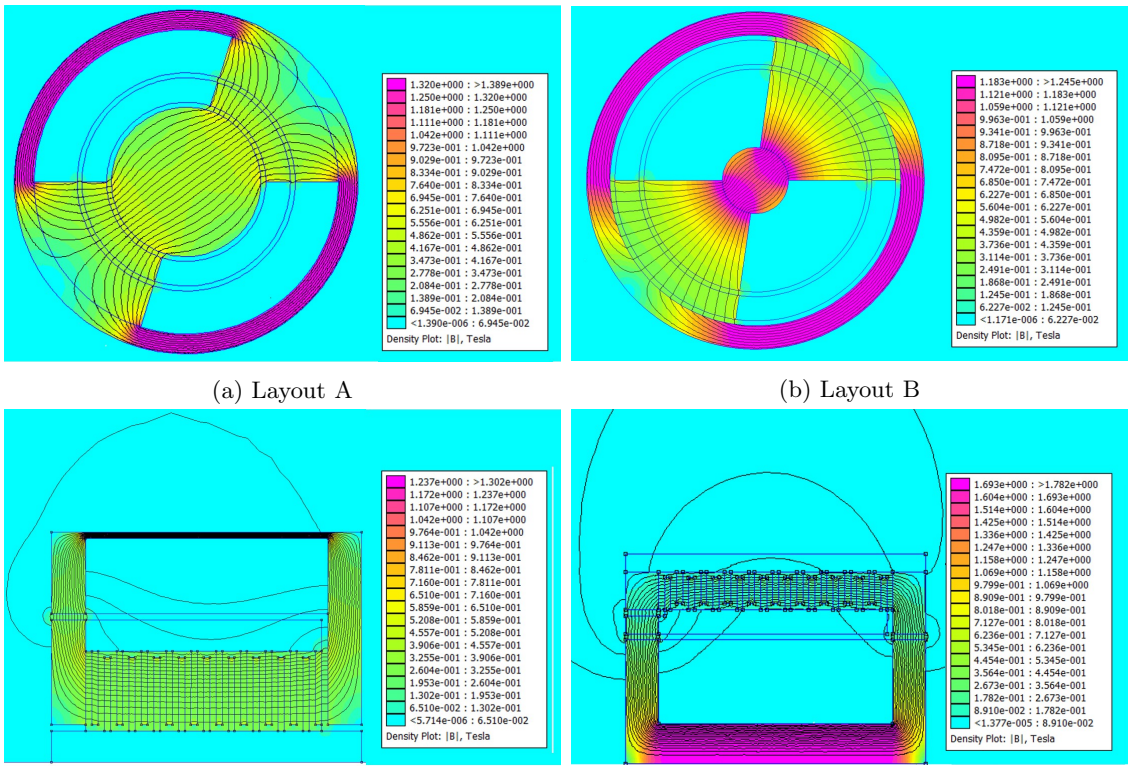

(a) Layout A (b) Layout B

(c) Layout C (d) Layout D

Figure 9: Magnetic flux density FEM model results.

Layout	Lumped parameters model(T)	FEM model (T)
a)	0.56	0.51
b)	0.34	0.30
c)	0.26	0.30
d)	0.31	0.17

Table 3: Magnetic flux density comparison.

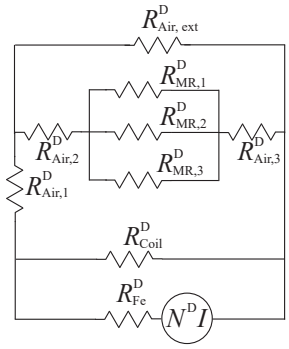

Figure 10: Magnetic circuit modification - Layout D

Indeed, many flux lines disperse in the external air and also in the coil volume, causing a significant reduction of the magnetic flux through the fluid.

7 Lumped parameters model improvement

For this reason, an improved magnetic circuit model is proposed in Fig. 4, which takes into account also the reluctance of the coils volume R^D_{coils} and of the external air $R^D_{air,ext}$, defined as follows,

$$R^D_{coils} = \frac{l - 2d^D}{\pi\mu_0((r^D_2)^2 - (r^D_1)^2)} \tag{41}$$

$$R^D_{air,ext} = k\frac{l - 2d^D}{\pi\mu_0((r^D_5)^2 - (r^D_4)^2)} \tag{42}$$

was implemented. Since no precise dimension can be associated to the area of the external air tube of flux, the dimension of the external ferromagnetic hollow cylinder was considered and multiplied by k which is a tunable parameter and was set to 0.1 after some iterations, where the results obtianed by the lumped parameter model varying k were compared to those given by the FEM model.

The optimal parameters found using this new model are listed in Tab. 4 and these are compared with the ones related to the original model. It is worth noting that no geometrical parameter varies in a significative way, while the magnetic field and the magnetic flux density in the fluid strongly decreases. This is due to the fact that the MR fluid is crossed only by a part of the magnetic flux, while a residual part disperses in the air. However, since the geometrical parameters are almost unchanged even if a further optimization was performed using the new model, the original model can be considered satisfactory to find the optimal geometrical parameters, even if the magnetic

Parameter	New model	Original model
$\overline{T}^D$(Nm)	2.79	5.49
$\overline{n}^D$ (-)	10	10
$\overline{r}_1^D$ (mm)	7.53	6.7
$\overline{r}_2^D$ (mm)	19.9	20.7
$\overline{r}_3^D$	25.9	26.7
$\overline{r}_4^D$ (mm)	32	32
$\overline{d}^D$(mm)	5.5	5.5
$\overline{H}_{MR}^D$ (kA/m)	19.4	27.4
$\overline{B}_{MR}^D$ (T)	0.19	0.31
$\overline{N}^D$	321	362

Table 4: Comparison of the optimal parameters found used the original (Fig. 6c) and the new magnetic circuit model (Fig. 4) - Layout D

Layout	New lumped parameters model(T)	FEM model (T)
d)	0.19	0.18

Table 5: Magnetic flux density comparison.

field computation and, consequently, the torque computation is not exact.

Figure 11 shows the results of the FEM model validation of the geometry found using the new model and Tab. 5 show the comparison between the new lumped parameter model and the FEM model: the error is strongly reduced, confirming that the new model correctly reproduces the actual magnetic circuit.

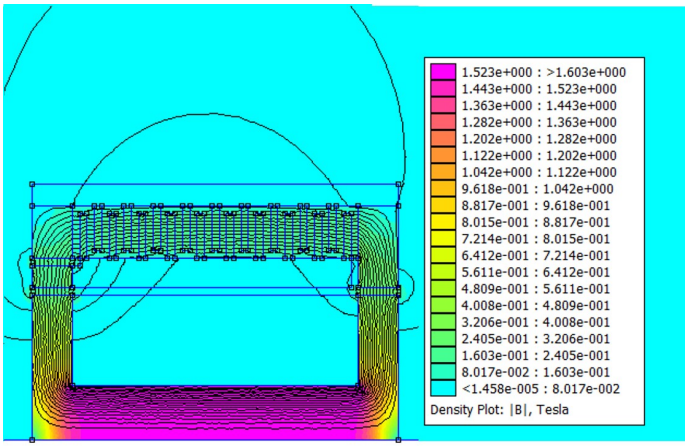

Figure 11: Magnetic flux density FEM model results - Layout D, New model

8 Conclusions

The magnetic optimization of a magnetorheological clutch has been discussed in the paper. The optimization was based on a simplified representation, i.e. described by a lumped parameters model, of the clutch, considering four different layouts. The optimization was conceived in order to find the optimal geometry (maximum torque) under size, topological consistency and magnetic saturation of the iron constraints.

As discussed in the paper, the simplified representation can be easily implemented and, being time-saving, resulted particularly advantageous for the optimization process. Critical parameters for the lumped parameters model are the relative reluctances of the different materials and the clear existence of preferred low reluctance paths for the magnetic flux. It has been discussed that the transmitted torque determined by the lumped parameter model gave satisfactory agreement with a more accurate representation of the clutch, given by a 2D FEM model, with error within 10%, in three of the examined cases where the magnetic flux is confined in the ferromagnetic material and do not disperse in air or in the coils. For one of the considered geometries, the setup of a more accurate model was necessary, due to the dispersion of a portion of the magnetic flux passing through the air and coils.

In all cases the optimization procedure based on the simplified lumped parameter model revealed capable of giving a correct estimate of the dimensions of the main components of the clutch, even if the torque could be overestimated in case of magnetic flux dispersion in air or coils.

References

[1] E. Bingham. An investigation of the laws of plastic flow. *U.S. Bureau of Standards Bulletin*, 13:309–353, 1916.

[2] W. Herschel and R. Bulkley. Konsistenzmessungen von gummi-benzollsungen. *Kolloid Zeitschrift*, 39:291–300, 1926.

[3] Mark R Jolly, Jonathan W Bender, and J David Carlson. Properties and applications of commercial magnetorheological fluids. *Journal of intelligent material systems and structures*, 10(1):5–13, 1999.

[4] Norman Wereley. *Magnetorheology: advances and applications*, volume 6. Royal Society of Chemistry, 2013.

[5] Huseyin Sahin, Faramarz Gordaninejad, Xiaojie Wang, and Yanming Liu. Response time of magnetorheological fluids and magnetorheological valves under various flow conditions. *Journal of Intelligent Material Systems and Structures*, 23(9):949–957, 2012.

[6] Chang Sheng Zhu. The response time of a magnetorheological fluid squeeze film damper rotor system. In *Key Engineering Materials*, volume 334, pages 1085–1088. Trans Tech Publ, 2007.

[7] J. Rabinow. The magnetic fluid clutch. *AIEE Transactions*, pages 1308–1315, 1948.

[8] J. Rabinow. Magnetic fluid torque and force transmitting device. *U.S. Patent*, page 2575360, 1951.

[9] J. de Vicente, D. J. Klingenberg, and R. Hidalgo-Alvarez. Magnetorheological fluids: a review. *Soft Matter*, 7(8):3701–3710, 2011.

[10] A.G. Olabi and A. Grunwald. Design and application of magneto-rheological fluid. *Materials & design*, 28(10):2658–2664, 2007.

[11] J. D. Carlson. MR fluids and devices in the real world. *International Journal of Modern Physics B*, 19(07n09):1463–1470, 2005.

[12] X. Zhu, X. Jing, and L. Cheng. Magnetorheological fluid dampers: a review on structure design and analysis. *Journal of Intelligent Material Systems and Structures*, 23(8):839–873, 2012.

[13] F. Gordaninejad and S. P. Kelso. Magneto-rheological fluid shock absorbers for HMMWV. In *SPIE's 7th Annual International Symposium on Smart Structures and Materials*, pages 266–273. International Society for Optics and Photonics, 2000.

[14] F. Gordaninejad and S. P. Kelso. Fail-safe magneto-rheological fluid dampers for off-highway, high-payload vehicles. *Journal of Intelligent Material Systems and Structures*, 11(5):395–406, 2000.

[15] S.R. Hong, G. Wang, W. Hu, and N.M. Wereley. Liquid spring shock absorber with controllable magnetorheological damping. *Proceedings of the Institution of Mechanical Engineers, Part D: Journal of Automobile Engineering*, 220(8):1019–1029, 2006.

[16] Z.X. Li and L.H. Xu. Performance tests and hysteresis model of MRF-04K damper. *Journal of Structural Engineering*, 131(8):1303–1306, 2005.

[17] B.M. Kavlicoglu, F. Gordaninejad, C.A. Evrensel, N. Cobanoglu, Y. Liu, A. Fuchs, and G. Korol. High-torque magnetorheological fluid clutch. In *SPIE's 9th Annual International Symposium on Smart Structures and Materials*, pages 393–400. International Society for Optics and Photonics, 2002.

[18] W.H. Li and H. Du. Design and experimental evaluation of a magnetorheological brake. *The International Journal of Advanced Manufacturing Technology*, 21(7):508–515, 2003.

[19] V.A. Neelakantan and G.N. Washington. Modeling and reduction of centrifuging in magnetorheological (MR) transmission clutches for automotive applications. *Journal of Intelligent Material Systems and Structures*, 16(9):703–711, 2005.

[20] G.L. Johnston, W. C. Kruckemeyer, and R.E. Longhouse. Passive magnetorheological clutch, December 15 1998. US Patent 5,848,678.

[21] T. Saito and H. Ikeda. Development of normally closed type of magnetorheological clutch and its application to safe torque control system of human-collaborative robot. *Journal of Intelligent Material Systems and Structures*, 18(12):1181–1185, 2007.

[22] B. Yang, T. Chen, G. Meng, Z. Feng, J. Jiang, S. Zhang, and Q. Zhou. Design of a safety escape device based on magnetorheological fluid and permanent magnet. *Journal of intelligent material systems and structures*, page 1045389X12459589, 2012.

[23] F. Bucchi, P. Forte, F. Frendo, A. Musolino, and R. Rizzo. A fail-safe magnetorheological clutch excited by permanent magnets for the disengagement of automotive auxiliaries. *Journal of Intelligent Material Systems and Structures*, page 1045389X13517313, 2014.

[24] R. Rizzo, A. Musolino, F. Bucchi, P. Forte, and F. Frendo. A multi-gap magnetorheological clutch with permanent magnet. *Smart Materials and Structures*, 24(7):075012, 2015.

[25] F. Bucchi, P. Forte, A. Franceschini, and F. Frendo. Analysis of differently sized prototypes of an MR clutch by performance indices. *Smart Materials and Structures*, 22(10):105009, 2013.

[26] K. Karakoc, E.J. Park, and A.l Suleman. Design considerations for an automotive magnetorheological brake. *Mechatronics*, 18(8):434–447, 2008.

[27] Q.H. Nguyen and S.B. Choi. Optimal design of an automotive magnetorheological brake considering geometric dimensions and zero-field friction heat. *Smart Materials and Structures*, 19(11):115024, 2010.

[28] P.B. Nguyen and S.B. Choi. A new approach to magnetic circuit analysis and its application to the optimal design of a bi-directional magnetorheological brake. *Smart Materials and Structures*, 20(12):125003, 2011.

[29] Q.H. Nguyen and S.B. Choi. Optimal design of a novel hybrid mr brake for motorcycles considering axial and radial magnetic flux. *Smart Materials and Structures*, 21(5):055003, 2012.

[30] Q.H. Nguyen and S.B. Choi. Selection of magnetorheological brake types via optimal design considering maximum torque and constrained volume. *Smart Materials and Structures*, 21(1):015012, 2011.

[31] Q.H. Nguyen, N.D. Nguyen, and S.B. Choi. Design and evaluation of a novel magnetorheological brake with coils placed on the side housings. *Smart Materials and Structures*, 24(4):047001, 2015.

[32] Francesco Bucchi, Paola Forte, and Francesco Frendo. Temperature effect on the torque characteristic of a magnetorheological clutch. *Mechanics of Advanced Materials and Structures*, 22(1-2):150–158, 2015.

[33] J.A. Nelder and R. Mead. A simplex method for function minimization. *The computer journal*, 7(4):308–313, 1965.

[34] D. Meeker. Finite element method magnetics. *FEMM*, 4:32, 2010.

[35] Konstantinos B Baltzis. The finite element method magnetics (FEMM) freeware package: May it serve as an educational tool in teaching electromagnetics? *Education and Information Technologies*, 15(1):19–36, 2010.